Formation of iron-carbonate scale-layer and corrosion mechanism of API X70 pipeline steel in carbon dioxide-saturated 3% sodium chloride

J. Hernandez, A. Muñoz and J. Genesca*
Dpto. Ingeniería Metalúrgica. Facultad Química. UNAM. Ciudad Universitaria.
04510 México D.F.

Efecto de la formación de una capa de carbonato de hierro en el mecanismo de corrosión de un acero API X70 en una solución de cloruro de sodio al 3% saturada con dióxido de carbono

Efecte de la formació d'una capa de carbonat de ferro en el mecanisme de corrosió d'un acer API X70 en solució de clorur de sodi al 3% saturada de diòxid de carboni

Recibido: 2 de agosto de 2012; aceptado: 17 de octubre de 2012

RESUMEN

En este trabajo se presentan los resultados obtenidos durante el estudio de la corrosión de un acero grado API X70 sumergido en una solución de NaCl al 3% saturada con CO_2 a una temperatura de 20°C bajo condiciones de flujo laminar y turbulento. Para controlar las condiciones hidrodinámicas del sistema se ha utilizado un electrodo de cilindro rotatorio, ECR. Dos técnicas electroquímicas, resistencia de polarización lineal y curvas de polarización han sido utilizadas para determinar el efecto del flujo turbulento en la cinética de corrosión del acero estudiado.
Asimismo se ha determinado el efecto de la temperatura en la velocidad de corrosión del acero API X70 bajo las condiciones experimentales estudiadas, ya que frecuentemente la corrosión de éste en medios acuosos que contienen CO_2 conlleva la precipitación de carbonato de hierro, $FeCO_3$ como producto de corrosión. Las propiedades protectoras de esta capa incrustante de $FeCO_3$ formada en salmueras que contienen CO_2 se proponen como una posible causa de la disminución de la velocidad de corrosión por encima de 60°C.

Palabras clave: acero API X70, corrosión por CO_2, carbonato de hierro, curvas de polarización, electrodo de cilindro rotatorio

SUMMARY

This work presents the electrochemical results obtained during the study of the corrosion of X70 pipeline steel samples immersed in a 3 % wt NaCl solution saturated with CO_2 at 20 °C under static and controlled turbulent flow conditions. In order to control the hydrodynamic conditions of the system, a rotating cylinder electrode (RCE) was used. Electrochemical techniques, Linear Polarization Resistance (LPR) and polarization curves, were used to determine the effect of turbulent flow upon the corrosion kinetics of the steel.
We also elucidate the effect of temperature on the corrosion rate of the API X70 steel under the experimental conditions studied. Often, the corrosion of carbon steel in aqueous environments containing CO_2 involves the formation of solid iron carbonate, $FeCO_3$, as a corrosion product. The protective property of the formed $FeCO_3$ scale layer to corrosion in brine solutions containing CO_2 was established as the possible cause of the corrosion rate decrease above 60 °C._

Keywords: API X70 steel, CO_2 corrosion, iron carbonate, polarization curves, rotating cylinder electrode

RESUM

Es presenten els resultats obtinguts en l'estudi de la corrosió d'un acer grau API X70 submergit en una solució de NaCl al 3% saturada de CO_2 a temperatura ambient sota les condicions de règim laminar i turbulent. Per tal de controlar les condicions hidrodinàmiques del sistema estudiat s'ha emprat un electrode de cilindre rotatori, ECR. Dues tecniques electroquímiques, resistencia de polarització lineal i corbes de polarització han estat emprades per determinar l'efecte del règim turbulent en la cinética de corrosió de l'acer estudiat.
Aixi mateix s'ha determinat l'efecte de la temperatura sobre la velocitat de corrosió de l'acer API X70 sota les condicions experimentals estudiades, ja que amb molta frequencia la corrosió d'aquest en medi aquós saturat amb CO_2 produiex la precipitació de carbonat de ferro, $FeCO_3$ com a producte de corrosió. Les propietats protectores d'aquesta capa incrustant de $FeCO_3$ que es forma en salmorres que contenen CO_2 son proposades com una possible causa que permet explicar la disminució de la velocitat de corrosió per damunt dels 60°C.

Paraules clau: acer API X70, corrosió per CO_2, carbonat de ferro, corbes de polarització, electrode de cilindre rotatori.

*Autor para la correspondencia: genesca@unam.mx

INTRODUCTION

Carbon dioxide, CO_2, corrosion is frequently found on the steel pipelines and process equipment used in the extraction, production and transport of oil and gas. This form of metal degradation is very common when carbon steel corrodes in brines containing CO_2. The presence of CO_2 causes internal "sweet" corrosion due to the formation of corrosive carbonic acid, H_2CO_3, in a low resistivity environment. This carbonic acid significantly increases corrosion rates on carbon steel pipelines. Corrosion rate depends, to a great extent, on the environmental conditions involved, such as pH, temperature, pressure, solution chemistry, flow and metallurgy of the steel, and surface films.

The mechanistic model for CO_2 corrosion of mild steel has been recently reviewed by Nesic et al. [1-3]. Many years ago, de Waard and Milliams [4] proposed a corrosion mechanism for steel in CO_2 solutions involving the direct reduction of carbonic acid as the dominant cathodic mechanism. For the anodic reaction the Bockris mechanism [5] for iron dissolution was proposed. Nesic et al. [6] have questioned some of the underlying assumptions made in this first model.

The Rotating Cylinder Electrode (RCE) is a tool that allows study under controlled turbulent flow conditions [7-9]. It has a well-defined hydrodynamic behaviour and a uniform distribution of current [8-11]. The RCE also has some practical advantages such as the need of relatively small quantities of test fluid and ease of cleaning [12]. Several studies have used the RCE to determine the influence of turbulent flow on the corrosion rate [13-16].

Oil and gas wells that contain CO_2 as the primary corrosive gas are termed "sweet" wells. The effect of CO_2 on corrosion is generally related to its partial pressure. The CO_2 concentration in the water phase can vary significantly within an individual well at different depths because of the large changes in temperature and pressure.

This work reports the influence of the turbulent flow on the corrosion of API X70 pipeline steel samples immersed in aqueous solutions containing dissolved CO_2 as well as the possible effect of iron carbonate ($FeCO_3$) formation on its corrosion behavior.

EXPERIMENTAL

All electrochemical experiments were carried out at 20°C and at the atmospheric pressure of Mexico City (0.7 bar). The aqueous test solution was a 3.5 % NaCl brine. In order to remove oxygen from the solution, N_2 gas (99.99%) was bubbled into the test solution for a period of 40 minutes. Immediately after oxygen removal CO_2 gas (99.99%) was bubbled into the solution until saturation was reached, P_{CO2} = 0.7 bar (atmospheric pressure). The theoretical saturation pH of the NaCl brine was 3.9. This pH value was experimentally measured and good agreement between theoretical and experimental values was observed. No significant increase on the pH value was observed from the release of iron.

All the electrochemical measurements were carried out in a 1 L, air-tight three-electrode, electrochemical glass cell. Cylindrical working electrodes were used in all experiments. These cylinders were machined from a pipeline steel API 5L X70 rods. Chemical composition of this steel was determined to be as follows: 0.037 % C, 1.49 % Mn, 0.0098 % P, 0.0036 % S, 0.098 % Nb, 0.037 % Mo. The microstructure of the steel samples indicated that this material had been quenched and tempered. A new clean sample was always used for each experiment and prior to the electrochemical tests the samples were polished with SiC paper up to 800 grit, rinsed with deionised water, degreased with acetone, and then kept in a desiccator until used. For static conditions, the total exposed area of the test specimen was 5.68 cm^2 and 3.4 cm^2 for dynamic conditions. As a reference a saturated calomel electrode (SCE) was used. A sintered graphite electrode was used as an auxiliary electrode. Hydrodynamic conditions were controlled using a Princeton Applied Research Model 636 Rotating Cylinder Electrode (RCE) system (RCE diameter 1.2 cm). The rotation rates studied were: 100, 1000, 2000, 3000, 4000, and 5000 rpm.

For all electrochemical studies an ACM Instruments Gill potentiostat was used. Linear polarization resistance (LPR) and potentiodynamic polarization curve tests were carried out at selected time intervals during a 24-hour exposure period. All electrochemical tests were carried out on clean samples and in freshly prepared test solutions.

Potentiodynamic LPR was used with a potential range of ± 0.015 V with respect to E_{corr}, the sweeping rate was 1 mV s^{-1}. Potentiodynamic polarization curves were also recorded at a sweeping rate of 1 mV s^{-1}.

The sequence used in the experimentation was: once the CO_2 solution reached a stable pH (3.9), the API steel electrode fitted on the RCE was immersed and rotated at the desired rate. During the experiment E_{corr}, R_p and polarization curves were measured at various immersion times.

In order to assure good reproducibility, experiments were repeated several times. Selected experiments are presented here in order to show the relevant effects.

Corrosion rate was determined by the weight loss of API X70 steel samples in a stagnant 3.5% NaCl solution containing CO_2. Gravimetric tests were conducted at atmospheric pressure in a cell at different temperatures, 25 to 75 °C. After each test the samples were chemically cleaned to remove the scale and weighed to determine the corrosion rate.

RESULTS AND DISCUSSION

3.1 The Effect of Hydrodynamics on Corrosion

The effect of hydrodynamics on the corrosion of X70 API steel in a flowing CO_2 saturated 3 % NaCl brine at a temperature of 20 °C was studied at pH = 3.9 on a rotating cylinder electrode system under a variety of hydrodynamic and mass transfer conditions.

Figure 1 shows the variation of measured corrosion potential, E_{corr} , of the tested API steel, at different rotation rates of the RCE. The E_{corr} values show a clear tendency to increase towards higher anodic potential as immersion time increases. The E_{corr} reaches a steady-state value after approximately 500 s. This shift towards higher anodic potential can be explained by the possible formation of an iron carbonate film. The measured E_{corr} values are affected by the rotation rate of RCE. For the steel tested, and for the rotation rate range studied, E_{corr} shows a clear tendency to be more anodic as the rotation rate increases. This shift to higher anodic potential can be explained by the effect of flow on the cathodic diffusion current.

Polarization curves for the X70 steel are shown in Figure 2. This shows the polarization curves measured at rotation rates of 0, 100, 1000, 2000, 3000, and 5000 rpm. These polarization curves were obtained in a 3% NaCl solution saturated with CO_2 at the natural saturation pH, 20 °C, and a partial pressure of CO_2 equal to 0.7 bar. The natural saturation pH measured in the test solution was on the order of 3.9.

The polarization curves shown in Figure 2 indicate that, in general, a good reproducibility was obtained in the experimental results. Referring to the anodic branch of the polarization curves, three main regions can be observed:

One first region developing from the E_{corr} to potential values of – 0.5 V (SCE).

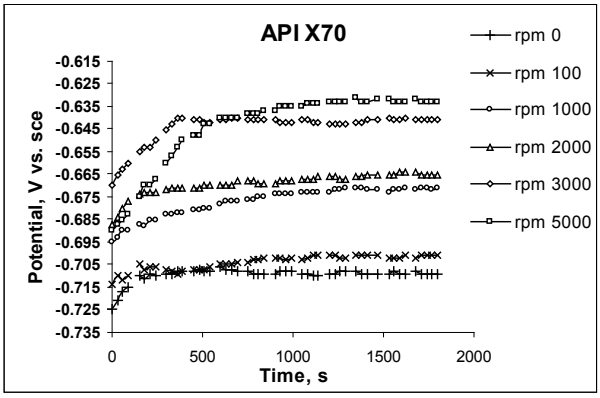

Figure 1. *Corrosion potential of the API X70 steel as a function of rotation rate. 3% NaCl solution saturated with CO_2, pCO_2 = 0.7 bar, pH = 3.9, 20 °C.*

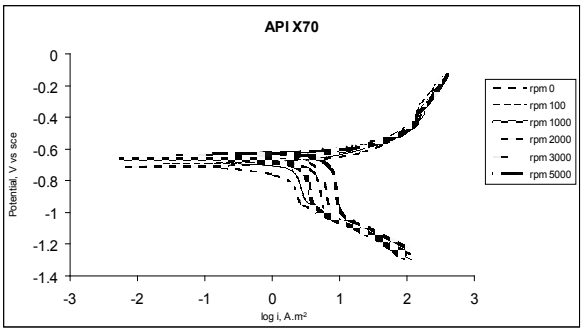

Figure 2. *Polarization curves at different rotation rates of API X70 steel. 3% NaCl solution saturated with CO_2, pCO_2 = 0.7 bar, pH = 3.9, 20 °C.*

A second region, in which a sudden change on the slope of the anodic current occurs, between – 0.50 to – 0.40 V (SCE),

A third region at higher anodic potentials, where another change in the slope of the anodic curve can be observed. This region can be seen above – 0.40 V (SCE).

These features can be explained in a qualitative manner as follows. As the potential of the working electrode increases from E_{corr}, an anodic reaction on the steel surface occurs and a linear relationship between the applied potential and the logarithm of the current density can be observed. This behavior corresponds to a charge-transfer process known as Tafel region, characterized by a slope (Tafel slope) that contains mechanistic information about the corrosion reaction. The region where a sudden change on the slope of the anodic polarization curve occurs, with a decrement in the anodic current, can be attributed to the formation of a passivating film. In CO_2 - containing solutions, free of dissolved oxygen, this film could be due to the formation of a $FeCO_3$ layer on the metal surface. At higher anodic potentials the resulting anodic current density increases again. This may be attributed to the growth of the film previously formed.

There is no apparent effect of flow on the anodic polarization curve. Then, for the two observed processes, the charge-transfer and the formation of a $FeCO_3$ film, a two-step mechanism can be proposed:

$$Fe \Rightarrow Fe^{2+} + 2\ e^- \quad (1)$$

$$Fe^{2+} + CO_3^{2-} \Rightarrow FeCO_3 \quad (2)$$

At the pH of the experiment, 3.9, the carbonate ion (CO_3^{2-}) is a minority species. Thus HCO_3^- can be regarded as the precipitable ion [17]:

$$HCO_3^- \Leftrightarrow H^+ + CO_3^{2-} \quad \text{where pK} = 10.3 \quad (3)$$

Then, the formation of $FeCO_3$ can occur according to

$$Fe^{2+} + HCO_3^- \Leftrightarrow FeCO_3 + H^+ \quad (4)$$

and an equilibrium constant, K, can be defined:

$$K = \frac{[H^+]}{[Fe^{2+}][HCO_3^-]} \quad (5)$$

It is clear that $FeCO_3$ precipitation is a function of pH, Fe^{2+} and HCO_3^- concentrations.

When CO_2 gas is in contact with water, several chemical equilibrium take place:

CO_2 gas ($CO_{2(g)}$) can be dissolved in water ($CO_{2(aq)}$) according to:

$$CO_{2(g)} \Rightarrow CO_{2(aq)} \quad (6)$$

the dissolved $CO_{2(aq)}$ can react with water forming the corresponding carbonic acid, H_2CO_3, according to the following reaction, known as a hydration reaction

$$CO_{2(aq)} + H_2O \Leftrightarrow H_2CO_3 \quad (7)$$

The hydration constant defined by the above equilibrium, K_{hyd}, varies only slightly with temperature. A value of 2.58 x 10^{-3} at 20 °C has been determined for this constant [18]. This small value means that the CO_2 hydration can be considered as a slow process and may, therefore, be the rate-determining step for subsequent reactions [19].

Once the H_2CO_3 is formed, it can dissociate according to:

$$H_2CO_3 \Leftrightarrow H^+ + HCO_3^- \quad (8)$$

The dissociation constant value for this reaction [19], K_{a1} is 1.74 x 10^{-4} mol dm^{-3}. The dissolution of CO_2 gas and the hydration reactions are both pH-independent. At acid values of pH, of the order of 3.9, the main carbonic species in solution is the bicarbonate ion, HCO_3^-.

Mora and Turgoose [17] proposed another possible formation route of $FeCO_3$:

$$Fe + H_2CO_3 \Leftrightarrow FeCO_3 + 2\ H^+ + 2\ e^- \quad (9)$$

To define whether it is possible that $FeCO_3$ could be formed via this reaction, Mora and Turgoose [17] calculated the corresponding equilibrium potential, $E_{Fe}/_{FeCO3}$. They found a value for the equilibrium potential $E_{Fe}/_{FeCO3} = -0.651$ V vs. SCE for pH 3.8. When this potential is compared with the E_{corr} in Figure 1, it can be noticed that $E_{Fe}/_{FeCO3}$ is similar to E_{corr} values, corresponding to turbulent flow conditions. This suggests that $FeCO_3$ may be stable with respect to metallic iron under these experimental conditions and it can be formed directly from equilibrium (9). Thus, it is possible to suggest that $FeCO_3$ films could continuously form, although they could also dissolve in their outer layer in contact with the bulk solution, as dictated by equilibrium (4) [17].

Rajappa et al. [20] have shown that $FeCO_3$ precipitation kinetics is extremely temperature-sensitive. At low temperatures (< 60 °C) $FeCO_3$ does not adhere to the surface and is transported away from the surface by fluid movement. Dugstad [21] found that protective films are not easily formed as the precipitation rate of $FeCO_3$ is a slow and temperature-dependent process. Also, under supersaturated conditions, it takes 20 to 40 hours to cover the metal surface with the protective iron carbonate layer. Evidence that the corrosion product can be $FeCO_3$ in CO_2-saturated 5% NaCl at a temperature of 25 °C and at a pressure of 1 atm was reported by Al-Sayed [22]. Using X-ray diffraction (XRD) he discovered that $FeCO_3$ was the main corrosion product under those conditions, with the solution pH fixed at 6.5. At pH 3.9, but with all other conditions the same, no $FeCO_3$ was detected. Thus, pH appears to be a critical factor that must be defined as clearly as temperature when discussing the presence or absence of $FeCO_3$. Videm et al. [23] showed that the most important surface changes induced by corrosion of an initially smooth and uncorroded steel surface are the change of area of the reacting surface, carbide accumulation at the surface, formation of carbonate films and flow-induced removal of the corrosion films.

Nesic et al. [24] shed more light on the anodic reaction mechanism in CO_2 corrosion of mild steel. They used potentiodynamic sweep and galvanostatic measurements for their electrochemical studies. They found distinct but different anodic mechanisms for iron dissolution in CO_2 solutions for both pH < 4 and pH > 5. In the intermediate area there seems to be a transition from one mechanism to another.

Nesic et al. [25] explained the influence of the iron content in the corrosive medium. They found that if the iron content in the medium becomes higher only after an initial phase of corrosion leading to the formation of a porous cementite (Fe_3C) layer, then internal acidification prevents further precipitation of iron carbonate in contact with the metal. The layer is then unprotective, and even enormous amounts of supersaturation cannot subsequently render it protective.

The corrosion of steel by aqueous CO_2 -containing solutions produces deposits of iron-containing materials on the steel surface. The chemical composition of these deposits is a function of the temperature. Jasinski [26] proposed formation of iron carbide at room temperature. All of the deposits were loosely held to the surface. The source of the Fe_3C is probably the steel itself [26], because, under the experimental conditions used, the formation of Fe_3C from iron and carbon dioxide is thermodynamically not allowed [26]. Metallographic analyses of the steel samples tested, revealed a microstructure formed by α-Fe and Fe_3C among others. The observed persistence of Fe_3C must result from the corrosion process itself, which etches out the metallic iron, leaving iron carbide behind.

A kinetic interpretation would be as follows: the Fe_3C areas would support cathodic reaction of H_2 formation, because this reaction is more favored (higher exchange current density) than on α-Fe areas, accelerating dissolution of the anodic zones of the metal by accelerating the cathodic component of the net corrosion process.

In this work, it was found that corrosion products formed after 1 h of immersion at E_{corr} conditions were non-uniform and lacking compactness, with a smudge-like appearance, easily removed under flowing conditions. This is in good agreement with Johnson and Tomson [27] and Lotz and de Waard [28]. It has been suggested for many authors that the kinetics of $FeCO_3$ precipitation are important. At higher temperature, where the solution can become easily and rapidly supersaturated with $FeCO_3$, deposition is fast and occurs at many sites, resulting in a well-compacted structure. While at room temperature, it is thought that precipitation progresses less rapidly than the corrosion reactions and a flat grain-type appearance is produced [29].

As proposed previously by Nesic et al. [25] internal acidification prevents further precipitation of iron carbonate in contact with the metal. This can be understood if it is assumed that Fe^{2+} generation is more rapid than that of carbonate. Thus Fe^{2+} would tend to diffuse into the bulk solution. The local environment would not become supersaturated with Fe^{2+} and a high local pH would be expected. This is illustrated in Figure 3, where the local metal surface represents an anode covered by $FeCO_3$, with migration of CO_3^{2-} ions towards it, produced through possible cathodic reduction of HCO_3^-. Since the local environment is assumed not saturated with Fe^{2+}, the deposition of $FeCO_3$ would be sluggish and would result in grain formation with voids.

Acidification can be due to Fe^{2+} hydrolysis:

$$Fe^{2+} + H_2O = FeOH^+ + H^+ \quad (10)$$

This would then force the dissolution of $FeCO_3$:

$$FeCO_3 + 2\ H^+ = Fe^{2+} + H_2O + CO_2 \quad (11)$$

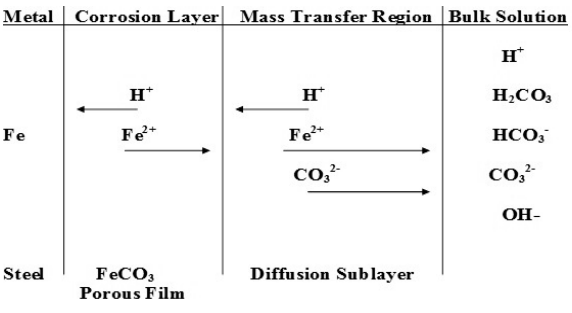

Figure 3. *Mass/transfer process at the steel/electrolyte interface with formation of $FeCO_3$ as the corrosion product layer [20].*

The anodic process (reaction (1)) corresponding to the electrochemical dissolution of iron in a water solution is the dominant reaction in CO_2 corrosion. This reaction is

controlled by a charge-transfer mechanism, thus it is free of mass transfer effects, as the anodic polarization curves clearly reflect. As noted by Nordsveen et al. [1] this reaction has been extensively studied in the past with several multistep mechanisms suggested to explain the various experimental results. The anodic dissolution in aqueous CO_2 solution has not been the subject of detailed mechanistic studies until recently [1]. The classic mechanism proposed by Bockris [30] has been assumed to apply in CO_2 solutions, in which the typical pH > 4. However, in the experiments presented here, the measured Tafel slopes were very different from the expected 30 to 40 mV. The measured values are always higher than 120 mV decade^{-1}. These values suggest that the metal surface could be covered by a film. Anodic dissolution of iron followed Tafel behavior for small overpotentials (slope 50-60 mV/decade) and was not flow sensitive.

In Table 1, the calculated values of the anodic Tafel slopes, b_a, are shown as a function of the rotation rate of the electrode. As can be observed, in general terms, as the rotation rate increases, the measured b_a remains relatively constant. This provides experimental evidence on the charge-transfer control of the anodic reaction, and therefore a mechanism that is not affected by flow.

Table 1. *Experimental Tafel slopes values for the API X70 steel in 3% NaCl solution containing CO_2*

Rotation Rate, rpm API X70	Anodic Tafel Slope, b_a, mV.decade^{-1}	Cathodic Tafel Slope b_c, mV.decade^{-1}
0	127	153
100	149	120
1000	137	136
2000	138	141
3000	159	125
5000	162	147

Concerning the cathodic branch of the polarization curves, the behavior is very different, as can be observed in Figure 2. These polarization curves were obtained on API X70 steel cylindrical samples at different rotation rates in a 3% NaCl solution saturated with oxygen-free CO_2 gas, at the natural pH of saturation, 3.9, and at a temperature of 20 °C.

Regarding the cathodic polarization curves, the following features can be observed in Figure 2. At all rotation rates a well-defined cathodic limiting current density, j_{lim}, region can be observed. This region is clearly affected by the rotation rate of the electrode and, in general, as the rotation rate increases the value of current density at which j_{lim} appear also increases. These facts can suggest that a diffusion-controlled process taking place on the surface of the electrode is being observed.

At lower cathodic potentials, below – 1.0 V (sce) approximately, the cathodic polarization curves overlap in a region of linear relationship between the potential of the electrode and the logarithm of the current density, log j. Also in this region, the measured current densities are not affected by the rotation rate. These features suggest that in this lower potential region, the electrochemical process that takes place on the electrode changes from a diffusion-controlled process to an activation-controlled process. The values of the calculated cathodic Tafel slopes, b_c, in this region are dependent on the data range considered. However, they are found to fall between –180 to – 200 mV decade^{-1}.

The different electrochemical reactions that can be responsible of the cathodic process are:

$$(a) \quad 2\,H^+ + 2\,e^- \Rightarrow H_2 \quad (12)$$

In CO_2 solutions, where typically pH ≥ 4, the presence of H_2CO_3 can increase the corrosion rate in two different ways [1]. Dissociation of H_2CO_3, as given by reaction (8) serves as an additional source of H^+ ions, which are subsequently reduced according to equation (12). In addition, there is a possibility that direct reduction of H_2CO_3 can increase the corrosion rate further:

$$(b) \quad 2\,H_2CO_3 + 2\,e^- \Rightarrow H_2 + 2\,HCO_3^- \quad (13)$$

Reduction of bicarbonate ions and hydrogen evolution by direct reduction of water requires a pH > 5, so it is not taken into consideration here.

If the expression for the RCE proposed by Eisenberg et al. [31] is considered and the values of limiting current densities, j_{lim} , are taken from Figure 2 at each rotation rate, and then plotted versus the rotation rate taken to the power 0.7, $\boldsymbol{u}_{RCE}^{0.7}$, Figure 4 is obtained. In this figure the rotation rate is expressed as peripheral velocity, $\boldsymbol{u}_{RCE}$.

The straight line represents a linear regression (LR) analysis on the averaged data. A very good reproducibility can be observed and the correlation coefficient of 0.98 calculated in the LR analysis indicates a perfect linear relationship of j_{lim} with the rotation rate taken to the power 0.7, $\boldsymbol{u}_{RCE}^{0.7}$.

This analysis shows that the measured j_{lim} is affected by the electrode rotation rate and follows the linear behavior predicted for the RCE proposed by Eisenberg et al. [31]. However, it must be noted that the intercept value of the calculated straight line is different to zero. This last feature can be thought as a flow-independent contribution to the total measured cathodic limiting current density.

3.2 Iron Carbonate Formation

Carbon steel can only by used in oil and gas production when the corrosion is effectively reduced by a layer of corrosion products, hydrocarbons or film inhibitors. Corrosion of carbon steel is influenced by a large number of parameters, as for example CO_2 and H_2S partial pressure, temperature, flow regime, microstructure, composition and surface condition of the steel. As a consequence of corrosion processes, a layer of corrosion products is formed on the surface of the steel. Its protection properties depend on the environmental conditions and the characteristics of the material. The presence of iron carbonate is commonly related with the formation of protective layers. Because of its low solubility (pK_{sp} = 10.54 at 25 °C) $FeCO_3$ precipitates when Fe^{2+} ions react with carbonate (CO_3^{2-}) and bicarbonate (HCO_3^-) ions in the solution.

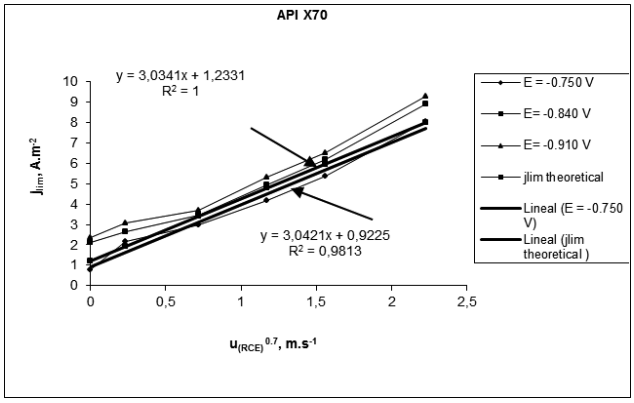

Figure 4 - *Limiting current densities as a function of the peripheral velocity of the electrode, $u_{(RCE)}^{0.7}$. 3% NaCl solution saturated with CO_2, pCO_2 = 0.7 bar, pH = 3.9, 20 °C.*

The surface scales formed below 40 °C in chloride media containing CO_2 consist mainly of cementite (Fe_3C) with some $FeCO_3$ and alloying elements of the steel. Fe_3C is part of the original steel microstructure and accumulates on the surface after the preferential dissolution of ferrite, α-Fe into Fe^{2+}. It is suggested that Fe_3C provides an available area for the cathodic reactions.

Corrosion rates as a function of temperature were measured by the weight-loss method as shown in Figure 5. Experiments were carried out in 3.5% NaCl stagnant solution saturated with CO_2. At low-temperature range, corrosion rate increases due to the continuous formation of Fe^{2+}. As temperature increases, at 60 °C approximately, the formed $FeCO_3$ film becomes more adherent to the metal surface and protective in nature, and hence the corrosion rate starts to decrease. Morphology of the attack (optical microscopy) could be observed after film removal. Samples showed localized corrosion at lower temperatures (25 to 55 °C), while at 75 °C the type of corrosion was uniform (generalized) and no occurrence of pitting was observed.

It has been reported that $FeCO_3$ precipitation is temperature-dependent, and that for its precipitation supersaturation with the Fe^{2+} ions is required, which is 5-10 times higher than the thermodynamically calculated values of solubility.

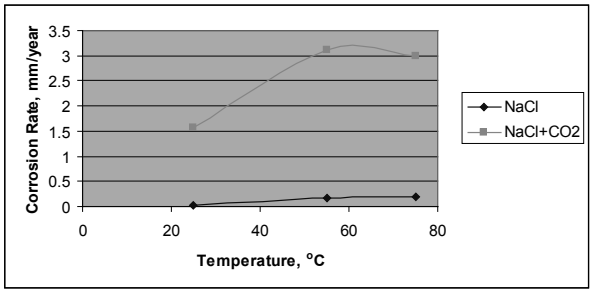

Figure 5. *Corrosion rate of X70 steel as a function of temperature. 3.5% NaCl solution saturated with CO_2. Stagnant conditions.*

The effects of solubility, precipitation and supersaturation of $FeCO_3$ have been studied in detail, and the most important findings have been published elsewhere [21]. Experiments have shown that precipitation of $FeCO_3$ is a slow, temperature-dependent process, and that a high degree of supersaturation can be maintained in a corroding system. The precipitation of $FeCO_3$ is facilitated by increased pH, increased temperature and measures that reduce the transport of reactants and corrosion products to and from the steel surface [32]. Nyborg and Dugstad [32] have pointed out that at low temperature the $FeCO_3$ solubility is high and the precipitation rate slow, and protective films will therefore not form unless the pH is artificially increased. At high temperature the $FeCO_3$ solubility is lower and the precipitation rate much faster, and very dense and protective iron carbonate films can form.

For the formation of a protective layer of $FeCO_3$ on the metal surface both a high pH and high temperature values, as well as $[Fe^{2+}]$ and $[CO_3^{2-}]$ exceeding the solubility limit, are required. Experiments were carried out at a pH of 6.6, temperature of 80 °C, with addition of $[Fe^{2+}]$ = 10 ppm, to facilitate the formation of a protective film of $FeCO_3$. Supersaturation values have been calculated with the following equation:

$$SS = \frac{[Fe^{2+}][CO_3^{2-}]}{[Ksp_{FeCO_3}]} \quad (14)$$

Then for pH 6.6, temperature of 80 °C, $[CO_3^{2-}] = 2.78*10^{-5}$ mol/l, and taking into account the ionic strength of the solution, $Ksp_{FeCO3} = 1.54*10^{-10}$, and for a $[Fe^{2+}]$ = 10 ppm ($1.79*10^{-4}$mol/l), a supersaturation value of SS = 32 can be calculated according to equation (14).

The precipitation of an homogeneous and dense film formed by the characteristic FeCO3 cubic crystals can be observed which make possible to suppose the formation of a thin, but protective layer. According to Figure 7, which shows a cross section of the $FeCO_3$ layer, the thickness of the film ranged from 2µm to 4µm. No evidence or sign of localized attack can be observed, in good agreement with the supposed protective nature of the film.

3.3 Corrosion Rate

The values of corrosion rates were determined by the Linear Polarization Resistance method (LPR). In each case, the value of the Stern-Geary constant was estimated taking into account the values of the Tafel slopes experimentally determined, see Table 1. These corrosion rate values were obtained on cylindrical rotating API X70 steel samples, in test solutions saturated with oxygen-free CO_2 gas.

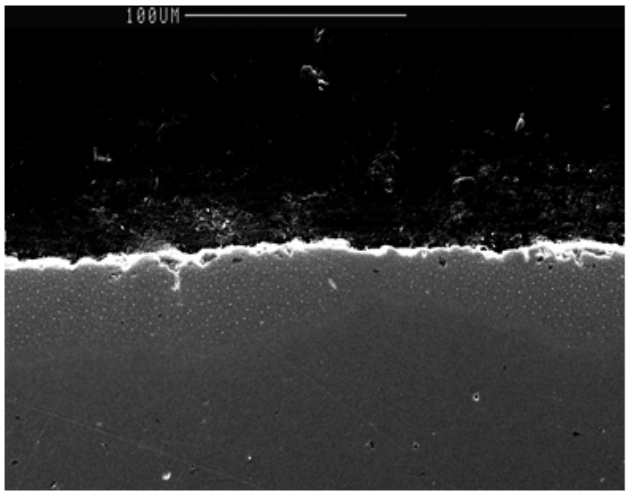

Figure 6. *SEM micrograph showing the cross section of the $FeCO_3$ layer formed on API X70 pipeline steel. Ex-*

perimental conditions: pH 6.6, 80 °C, SS = 32, [Fe^{2+}] = 10 ppm, 1000 rpm, CO_2 partial pressure of 0.7 bar, 400X.

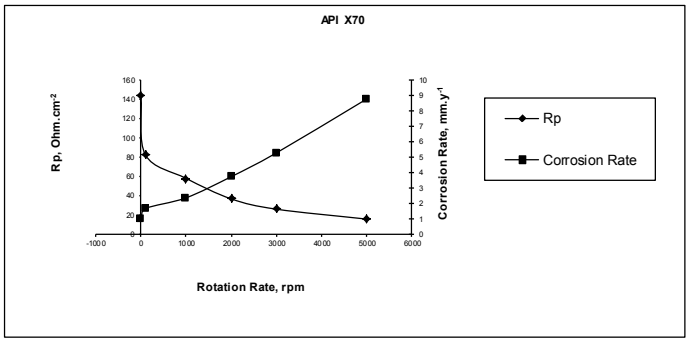

Figure 7. *Polarization resistance, R_p, and corrosion rate values of API X70 steel as a function of rotation rate. 3% NaCl solution saturated with CO_2, pCO_2 = 0.7 bar, pH = 3.9, 20 °C.*

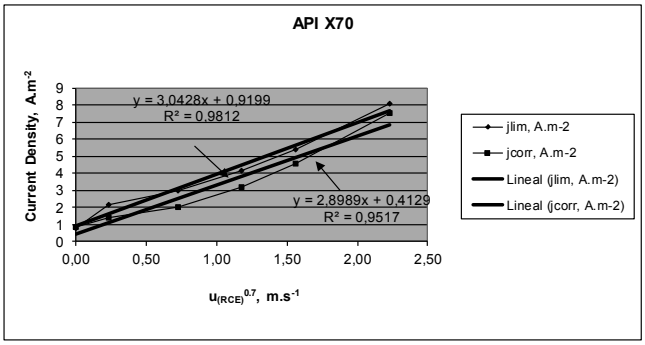

Figure 8. *Values of limiting current density, j_{lim}, , and corrosion current density, j_{corr}, obtained by the linear polarization resistance method, LRPM, as a function of the rotation rate taken to the power 0.7, $u_{(RCE)}^{0.7}$. API X70 grade steel in 3% NaCl solution saturated with CO_2, pCO_2 = 0.7 bar, pH = 3.9, 20 °C.*

Figure 7 shows the values of corrosion rates, expressed as polarization resistance R_p (Ω cm^2) and corrosion rate (mm $year^{-1}$) as a function of the rotation rate, u_{RCE} , measured at 20 °C. Polarization resistance values (R_p) measured at the CO_2 saturation pH show a clear dependence on the rotation rate. As the rotation rate of the electrode increases, R_p values clearly decrease.

These findings indicate that, at 20 °C, the corrosion process taking place on the surface of the electrode is dependent of the rotation rate. Therefor a mixed control by charge-transfer and mass-transfer on the overall corrosion process can be assumed. To understand the corrosion process taking place at the metal surface and to verify the measurements of corrosion current densities, a plot of these parameters vs. $u_{RCE}^{0.7}$ is presented in Figure 8. This was done to take into account the behavior predicted by the expression for the RCE proposed by Eisenberg et al. [31].

Figure 8 compares the measured values of j_{corr} with the measured values of cathodic limiting current densities, j_{lim} , as a function of $u_{RCE}^{0.7}$ at 20 °C and at the natural pH of saturation of the test solution. As Figure 8 shows, at rotation rates lower than 1.5 m s^{-1} and under the experimental conditions, the measured j_{corr} values are similar in magnitude to the measured values of j_{lim}. For all the rotation rate range studied, the measured values of j_{corr} exhibit a dependency on the rotation rate similar to the dependency exhibited by the measured values of j_{lim}. Then at 20 °C and at the natural pH of saturation of the test solution, the corrosion process taking place on the surface of the electrode exhibits a diffusion-control behavior. In general, the j_{corr} values are lower than the observed values of j_{lim}, but always showing a clear dependency with the rotation rate of the electrode.

CONCLUSIONS

At constant temperature and pH, the calculated anodic Tafel slope b_a is not a function of the rotation rate of the electrode.

Anodic dissolution of API X70 steel followed Tafel behavior for small overpotentials (slope 50-60 mV/decade) and was not flow sensitive.

Diffusion-limiting currents were observed which could be predicted by using mass-transfer correlations such as that of Eisenberg et al. [31] for a rotating cylinder electrode.

The corrosion rate under the experimental conditions studied, at 20 °C, natural pH of CO_2 saturation, pH 3.9, was under mixed control (activation-diffusion) and was flow sensitive.

At low temperatures the $FeCO_3$ film gets dissolved continuously and corrosion rate increases. At high temperatures a dense and more protective film of $FeCO_3$ can be formed and as a consequence a decrease in the corrosion rate results.

ACKNOWLEDGEMENT

The authors would like to thank the Mexican Science and Technology Council (CONACYT) for the grant awarded to A. Muñoz and J. Hernandez needed to develop this work.

BILIOGRAPHY

1. M. Nordsveen, S. Nesic, R. Nyborg, A. Stangeland, *Corrosion* **59** (5) 443 (2003).
2. S. Nesic, M. Nordsveen, R. Nyborg, A. Stangeland, *Corrosion* **59** (6) 489 (2003).
3. S. Nesic, K. L. J. Lee, *Corrosion* **59** (7) 616 (2003).
4. C. de Waard, D.E. Millliams, *Corrosion* **31** 131 (1975) .
5. J. O'M. Bockris, D. Drazic, A. R. Despic, *Electrochim. Acta* **4**, 325 (1961).
6. S. Nesic, J. Postlethwaite, S. Olsen, Corrosion/95, paper no. 131 (Houston, TX: NACE International, 1995).
7. D. C. Silverman, *Corrosion* **55** (12) 1115 (1999).
8. R. A. Holser, G. Prentice, R.B. Pond Jr., R. Guanti, *Corrosion* **46** (9) 764 (1990).
9. Corrosion 1, Metal/Environment Reactions, 3th Edition, L. L. Shreir, R. A. Jarman, G. T. Burstein. (Eds.), 1994, pp. 2:12-2:13.
10. D. R. Gabe, *J. Appl. Electrochem.* **4**, 91 (1974).
11. D. R. Gabe, *J. Appl. Electrochem.* **13**, 3 (1983).
12. ASTM G 170-01, Evaluating and Qualifying Oilfield and Refinery Corrosion Inhibitors in the Laboratory, NACE International, pp. 6-8 (1996).
13. D. C. Silverman, *Corrosion* **44** (1) 42 (1988).

14. V. Pérez-Herranz, M. T. Montañes, J. García-Antón, J. L. Guiñón, *Corrosion* **57** (10) 835 (2001).
15. K. D. Efird, E. J. Wright, J. A. Boros, T. G. Hailey, *Corrosion* **49** (12) 992 (1993).
16. B. Poulson, *Corros. Sci.* **23** (4) 391 (1983).
17. J. L. Mora-Mendoza, S. Turgoose, *Corros. Sci.* **44**, 1223 (2002).
18. D. A. Palmer, R. Van Eldik, *Chem. Rev.* **83** (6) 651 (1983).
19. J. Mendoza, PhD Thesis, UMIST, Corrosion and Protection Centre, Manchester, UK (1997).
20. S. Rajappa, R. Zhang, M. Gopal, Corrosion/98, paper no. 26 (Houston, TX: NACE International, 1998).
21. A. Dugstad, Corrosion/92, Paper no. 14 (Houston, TX: NACE, 1992).
22. M. S. A. Al-Sayed, Effect of Flow and pH on CO_2 Corrosion and Inhibition, PhD Thesis, UMIST, Manchester (1989).
23. K. Videm, J. Kvarekvaal, T. Perez, G. Fitzsimons, Corrosion/96, Paper no. 1 (Houston, TX: NACE International, 1996).
24. S. Nesic et al, Corrosion/95, Paper no. 131 (Houston, TX: NACE International, 1995).
25. S. Nesic, N. Thevenot, J. L. Crolet, D. Drazic, Corrosion/96, paper no. 3 (Houston, TX: NACE International, 1996).
26. R. Jasinski, *Corrosion* **43** (4) 214 (1987).
27. M. L. Johnson, M. B. Tomson, Corrosion/91, Paper no. 268 (Houston, TX: NACE, 1991).
28. U. Lotz, C. de Waard, Corrosion/91, Paper no. 577 (Houston, TX: NACE International, 1991).
29. H. Malik, *Corrosion* **51** (4) 321 (1995).
30. J. O'M. Bockris and A. N. Reddy, *Modern Electrochemistry*, Vol. II, (Plenum Press, New York, 1977).
31. M. Eisenberg, C. W. Tobias, C. R. Wilke, *J. Electrochem. Soc.* **101** (6) 306 (1954).
32. R. Nyborg and A. Dugstad, "Reliability and Limitations of Corrosion Prediction Tools for Oil and Gas Pipelines", Eurocorr/2004 (Nice: CEFRACOR, 2004).